Numerical simulations of confined Brownian motion

Elodie Millan, Maxime Lavaud, Yacine Amarouchene, Thomas Salez

Numerical simulations of confined Brownian motion

Elodie Millan,[1,*] Maxime Lavaud,[1,*] Yacine Amarouchene,[1,†] and Thomas Salez[1,‡]

[1] *Univ. Bordeaux, CNRS, LOMA, UMR 5798, F-33400, Talence, France.*

Brownian motion is a central scientific paradigm. Recently, due to increasing efforts and interests towards miniaturization and small-scale physics or biology, the effects of confinement on such a motion have become a key topic of investigation. Essentially, when confined near a wall, a particle moves much slower than in the bulk due to friction at the boundaries. The mobility is therefore locally hindered and space-dependent, which in turn leads to the apparition of so-called multiplicative noises. Here, we present efficient, broadrange and quantitative numerical simulations of a such a problem. Specifically, we integrate the overdamped Langevin equation governing the thermal dynamics of a negatively-buoyant spherical colloid within a viscous fluid confined by rigid walls, including surface charges. From the produced large set of long random trajectories, we perform a complete statistical analysis and extract all the key quantities, such as the probability distributions in displacements and their first moments. In particular, we propose a convenient method to compute high-order cumulants by reducing convergence problems, and employ it to characterize the inherent non-Gaussianity of the process.

I. INTRODUCTION

Brownian motion is the random movement of a microparticle due to thermal agitation. This name was given in reference to Robert Brown, a botanist, who observed in 1828 for the first time the erratic trajectories of pollen grains, using a microscope [1]. He concluded that this motion was not from a living source since he observed the same phenomenon with grains of inorganic matter, like minute fragments of window glass or mineral substances. In 1905, Albert Einstein [2], William Sutherland [3] and Marian Von Smoluchowski [4], physically modelled Brownian motion, and independently calculated the diffusion coefficient of a single particle, assuming that matter is discontinuous. In 1909, Jean Perrin [5] validated Einstein's theory by studying both the distribution and the agitation of microparticules in suspension. Moreover, doing so, he experimentally measured the Avogadro number, proving the atomic nature of matter, and was thus awarded the Nobel Prize in 1926. Besides, from this work, it then became clear that Brownian motion can be a probe of conservative forces. In 1908, Paul Langevin [6] developed the equation that governs Brownian trajectories using the fundamental principle of dynamics, and taking into account both the viscous Stokes force and a new stochastic force representing the effect of momentum transfer from collisions with solvent molecules. It is worth stressing that many variations and applications around Brownian motion in the bulk are continuously explored nowadays, and some of the key underlying hypotheses and concepts remain at the heart of epistemological discussions [7, 8].

In the second half of the 20th century, the rise of miniaturization triggered the need for further understanding interfacial and confinement effects on colloidal mobility [9–11]. Almost ninety years after the Einstein-Sutherland-Smoluchowski theory, a seminal study of Brownian motion near rigid walls was performed [12]. In the latter, the space-dependent wall-friction-induced reduction in the average planar diffusion coefficient of confined colloids was revealed. This result triggered a novel research activity on Brownian motion in confinement [13–19], with implications in single-molecule force spectroscopy [20, 21], surface-force measurements [22, 23], and single-algae motility analysis [24]. A key associated feature is the emergence of multiplicative noises and non-Gaussianity [25–44], despite the mean-square displacement (MSD) remains linear in time as expected for a classical Brownian process. Moving beyond rigid confinement at equilibrium, the influence of fluctuating interfaces on Brownian point-like tracers was investigated theoretically [45], and experimentally [46], as well as the effects of wall adhesion [47–49]. Besides, fluid and soft boundaries were considered [50–53], and Taylor dispersion in confinement was investigated [54–56].

While bulk Brownian motion has been modelled numerically (see *e.g.* Ref. [57] for a tutorial), efficient, broadrange and quantitative numerical simulations of confined Brownian motion allowing to characterize all the statistical quantities and revealing the non-Gaussian properties, are lacking to date. In this article, we aim at filling this gap. We describe how one can model the thermal dynamics of a negatively-buoyant spherical colloidal particle between two rigid walls, including surface charges. After recalling the overdamped Langevin equation including spurious forces, we solve it using an optimized numerical scheme, and investigate the full displacement statistics. We show in particular that special care needs to be taken in order to avoid convergence issues when computing high-order cumulants from Brownian realizations.

* These authors contributed equally.
† yacine.amarouchene@u-bordeaux.fr
‡ thomas.salez@cnrs.fr

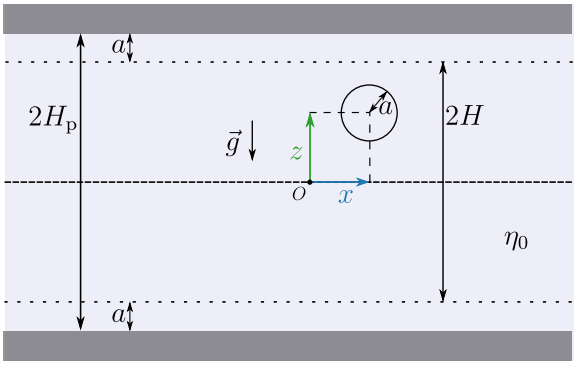

FIG. 1. Schematic of the system in the (x, y) plane. A surface-charged particule of radius a diffuses in three dimensions in a fluid of viscosity η_0, between two rigid, flat and surface-charged walls separated by a distance $2H_\mathrm{p} = 2H + 2a$.

II. MODEL

A. Bulk Langevin equation

We consider a colloidal particle of radius a, immersed in a fluid of dynamic shear viscosity η_0. In the bulk, the particle motion is described by the Langevin equation [6]:

$$m\ddot{\vec{r}}(t) = -\gamma\dot{\vec{r}}(t) + \vec{\mathcal{F}}(\vec{r}(t)) + \sqrt{2k_\mathrm{B}T\gamma}\ \vec{w}(t)\ , \quad (1)$$

where $\vec{r}(t) = [r_x(t), r_y(t), r_z(t)]$ is the particle center of mass position at time t, $m = \frac{4}{3}\pi a^3\rho$ is the particle mass, ρ is the particle density, $\gamma = 6\pi\eta_0 a$ is the bulk Stokes drag coefficient, k_B is the Boltzmann constant, T is the temperature, $\vec{\mathcal{F}} = -\vec{\nabla}V$ is the total conservative force deriving from the potential $V[\vec{r}(t)]$, and $\sqrt{2k_\mathrm{B}T\gamma}\ \vec{w}(t)$ is the stochastic Langevin force accounting for the random impacts of surrounding fluid molecules. In the following, the projected equations along x and y being independent and similar, we only consider the x axis. The two relevant spatial directions are thus indexed by $i = x, z$, corresponding to the coordinates $r_x(t) = x_t$ and $r_z(t) = z_t$. We model $\vec{w}(t) = [w_x(t), w_y(t), w_z(t)]$ as a Gaussian white noise of zero mean $\langle w_i(t)\rangle = 0$, and delta-correlated variance $\langle w_i(t)w_j(t')\rangle = \delta_{ij}\delta(t-t')$, where $\langle\cdot\rangle$ indicates the ensemble average, δ_{ij} the Kronecker symbol and δ the Dirac distribution.

The inertial term $m\ddot{\vec{r}}$ can be further neglected in the overdamped regime, which is reached when considering times greater than the inertial time scale $m/\gamma \approx 50$ ns, for $a = 1.5$ μm, $\rho = 1050$ kg.m^{-3} and $\eta_0 = 1$ mPa.s.

B. Overdamped Langevin equation in confinement

We now consider that the particle is confined between two rigid and flat walls separated by a distance $2H_\mathrm{p}$, as shown in Fig. 1. The gravitational acceleration $\vec{g}$ is oriented along $-z$. We further suppose that the particle and walls are negatively charged in water, inducing electrostatic interactions. In addition, the latter are screened by the ions present in water. Taking into account gravity and assuming a linear superposition of the Debye-Hückel screened electrostatic interactions from each wall, the total potential energy $V(z)$ reads:

$$\frac{V(z)}{k_\mathrm{B}T} = B\left[\mathrm{e}^{-(H+z)/l_\mathrm{D}} + \mathrm{e}^{-(H-z)/l_\mathrm{D}}\right] + \frac{H+z}{l_\mathrm{B}}\ , \quad (2)$$

where B is a dimensionless electrostatic magnitude related to the particle and wall surface-charge densities [58], l_D is the Debye length, $l_\mathrm{B} = k_\mathrm{B}T/(g\Delta m)$ is the Boltzmann length, and $\Delta m = m - \frac{4}{3}\pi a^3\rho_\mathrm{f}$ is the particle buoyant mass with ρ_f the fluid density.

Moreover, the presence of the walls modifies the particle mobilities in both the x and z directions, in an anisotropic fashion. Therefore, the Stokes drag coefficients now become space and direction dependent, and we note them $\gamma_i(z) = 6\pi a\eta_i(z)$, with $\eta_i(z)$ the local effective viscosities. Assuming a linear superposition of the contributions of each wall, one has [12, 59]:

$$\eta_i(z) \simeq \eta_i^{(1)}(H+z) + \eta_i^{(1)}(H-z) - \eta_0\ , \quad (3)$$

where we invoked the single-wall expressions $\eta_i^{(1)}$. The latter are given by the functional forms [9]:

$$\eta_x^{(1)}(u) = \eta_0\,\frac{1}{1 - \frac{9}{16}\xi + \frac{1}{8}\xi^3 - \frac{45}{256}\xi^4 - \frac{1}{16}\xi^5}\ , \quad (4)$$

with $\xi = a/(u+a)$, and:

$$\eta_z^{(1)}(u) = \eta_0\,\frac{6u^2 + 9au + 2a^2}{6u^2 + 2au}\ , \quad (5)$$

where the last expression is a Padé approximation [60] of the complete formula [9, 61], valid with less than 1% error. Invoking the Stokes-Einstein relation, we then construct the local diffusion coefficients, as:

$$D_i(z) = \frac{k_\mathrm{B}T}{\gamma_i(z)}\ . \quad (6)$$

For illustration, typical diffusion-coefficient profiles are show in Fig. 2(a) near the bottom rigid wall, and in Fig. 2(b) for two rigid walls.

We can then rewrite Eq. (1) in the overdamped regime for a particle between two rigid walls, as:

$$\begin{cases} \dfrac{\mathrm{d}x_t}{\mathrm{d}t} = \sqrt{2D_x(z_t)}\,w_x(t)\ , \\ \dfrac{\mathrm{d}z_t}{\mathrm{d}t} = \sqrt{2D_z(z_t)}\,w_z(t) + \dfrac{\mathcal{F}_z(z_t)}{\gamma_z(z_t)}\ , \end{cases} \quad (7)$$

with $\mathcal{F}_z(z_t) = -V'(z_t)$, where the prime indicates one derivative with respect to the argument. Eventually, at long time scales, the system must reach equilibrium, and one should recover the canonical Gibbs-Boltzmann distribution in position:

$$P_\mathrm{eq}(z) = \frac{\mathrm{e}^{-\beta V(z)}}{\int_{-H}^{+H}\mathrm{d}z'\,\mathrm{e}^{-\beta V(z')}}\ , \quad (8)$$

with $\beta = 1/(k_\mathrm{B}T)$.

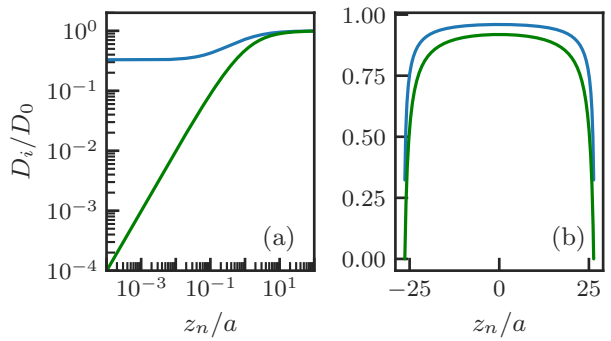

FIG. 2. Diffusion coefficients D_i along x (blue) and z (green), normalized by the bulk value $D_0 = k_B T/(6\pi a \eta_0)$[2], as functions of the rescaled discrete vertical coordinate z_n/a, as obtained from Eqs. (3,4,5,6), with $z_n = z_t$ for $t = n\delta t$. Two typical situations are considered: (a) near the bottom rigid wall, with the particle-wall contact point shifted here to correspond to $z_n = 0$; (b) between two rigid walls.

C. Spurious drift

One can observe that the noise magnitude $\sqrt{2D_i(z_t)}$ in Eq. (7) depends on the random variable z_t itself – a feature which is thus usually referred to as "multiplicative noise". It requires a specific treatment in stochastic calculus, the basics of which being recalled hereafter. Let us rewrite the vertical projection of Eq. (7) in a differential form, as:

$$\mathrm{d}z_t = [U(z_t) + A(z_t)w_z(t)]\mathrm{d}t \ , \tag{9}$$

with $A(z_t) = \sqrt{2D_z(z_t)}$, and where $U(z_t)$ is an unknown drift velocity at this stage. For integration, we consider a small time interval between t and $t+\tau$. Since there is an intrinsic ambiguity in the evaluation of A on this interval, we introduce a parameter $\alpha \in [0,1]$ that characterizes the chosen evaluation instant $t+\alpha\tau$. Note that there are two common conventions: i) $\alpha = 0$, *i.e.* the Îto convention; and ii) $\alpha = 1/2$, *i.e.* the Stratonovich convention. Imposing the steady state of the associated Fokker-Planck equation to be given by the Gibbs-Boltzmann distribution (see Eq. (8) for the marginal in position), one eventually gets for all conventions [62, 63]:

$$z_{t+\tau} = z_t + \left[\frac{\mathcal{F}_z(z_t)}{\gamma_z(z_t)} + (1-\alpha)A(z_t)A'(z_t) + A(z_t)w_z(t)\right]\tau \ , \tag{10}$$

where we have identified $U(z_t) = \mathcal{F}_z(z_t)/\gamma_z(z_t) + (1-\alpha)A(z_t)A'(z_t)$. By comparison with Eq. (7), we see the appearance of a convention-dependent spurious drift velocity $(1-\alpha)A(z_t)A'(z_t) = (1-\alpha)D_z'(z_t)$. Without this correction brought to the discretized overdamped Langevin equation, the simulated z_t realizations would not satisfy the Gibbs-Boltzmann distribution at long times. In the following, we choose the Îto convention ($\alpha = 0$).

D. Numerical simulations

We discretize the problem through an Euler scheme, by considering a discrete time $t = n\delta t$, with n a positive integer and δt the numerical time step. We write $r_i(t)$ as $r_{i,n}$, (x_t, z_t) as (x_n, z_n), and $w_i(t)$ as $w_{i,n}$. The discrete noises $w_{i,n}$ are chosen as independent Gaussian noises, each with zero mean and $1/\delta t$ variance. Specifically, to generate $w_{i,n}$, we first generate a pair of uniformly-distributed random numbers using the Mersenne-Twister generator [64]. Then, we transform the latter pair into a Gaussian-distributed random variable using the Box-Muller algorithm [65, 66]. From the discretization of the horizontal projection of Eq. (7), and from Eq. (10) for the vertical projection, we get the discrete overdamped Langevin equation in the Îto convention:

$$\begin{cases} x_{n+1} = x_n + \sqrt{2D_x(z_n)}w_{x,n}\delta t \\ z_{n+1} = z_n + [D_z'(z_n) - \beta D_z(z_n)V'(z_n) \\ \qquad\qquad + \sqrt{2D_z(z_n)}w_{z,n}]\delta t \ . \end{cases} \tag{11}$$

To ensure thermalization in the vertical direction, we enforce initial conditions $(x_0, z_0) = (0, z_0)$, with z_0 randomly sampled from the Gibbs-Boltzmann distribution of Eq. (8), using an inverse transformation sampling [67]. In the following, each particle trajectory is simulated with $\delta t = 0.01$ s, $a = 1.5$ μm, $\eta_0 = 1$ mPa.s, $B = 5.0$, $l_B = 526$ nm, and $l_D = 88$ nm, in order to reproduce a realistic experimental situation [23]. A typical trajectory is shown in Fig. 3(a), for the 1000 first seconds. To make sure that the equilibrium along the vertical direction is reached, we verify that the Gibbs-Boltzmann distribution of Eq. (8) is reached, without any free parameter, as shown in Fig. 3(b).

We run N_s simulations. Each simulation produces a trajectory of N_t points in time. The simulations are performed using *Python* [68], and each of these can take several seconds of real computation time for $N_t = 10^5$, as shown in Fig. 4. For $N_s = 2 \cdot 10^6$ trajectories with $N_t = 10^5$, we would need several months of real computation time. To reduce the computational time, we use *Cython* [69], which allows to keep the flexibility and ease of use of *Python*. As shown in Fig. 4, for $N_t > 10^4$, simulations using *Cython* are a hundred times faster than the ones using *Python*.

III. RESULTS

A. Mean square displacements

After having verified above that the simulated system reaches equilibrium properly, one can now turn to the investigation of the dynamical properties of interest. Let us start with the canonical and well-documented quantities, *i.e.* the Mean Squared Displacements (MSDs), which are

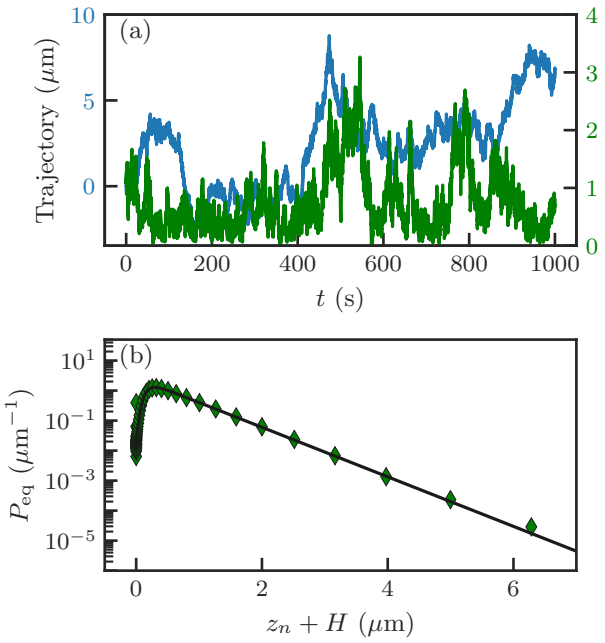

FIG. 3. (a) Typical numerically-simulated trajectory of a Brownian particle confined by two rigid walls, in presence of gravity and surface charges. The blue and green lines respectively represent x_n and $z_n + H$, for the first 10^5 points over a total of $N_{\rm t} = 10^8$ points, using a time step $\delta t = 0.01$ s. (b) Long-term distribution of the wall-particle distance $z_n + H$. The solid line corresponds to Eqs. (2) and (8), with $a = 1.5$ μm, $B = 5.0$, $l_{\rm B} = 526$ nm, $l_{\rm D} = 88$ nm, and $H_{\rm p} = 40$ μm.

defined as [70]:

$$\langle \Delta r_i^2 \rangle(\tau) = \langle [r_i(t+\tau) - r_i(t)]^2 \rangle \ , \tag{12}$$

where the ensemble average $\langle \cdot \rangle$ is computed in practice from an average $\langle \cdot \rangle_t$ over time t. At all time lags τ for the horizontal direction, and at small time lags for the vertical one, the MSDs are linear in τ, as shown in Fig. 5. Indeed, the absence of a preliminary ballistic regime is expected for the governing overdamped Langevin equation for (see Eq. (11)). In the bulk, one would have $\langle \Delta r_i^2 \rangle(\tau) = 2D_0\tau$. However, in the confinement situation at stake here, the prefactor is modified, and one expects instead:

$$\langle \Delta r_i^2 \rangle(\tau) = 2\langle D_i \rangle_0 \tau \ , \tag{13}$$

where $\langle \cdot \rangle_0 = \int_{-H}^{+H} {\rm d}z \, (\cdot) P_{\rm eq}(z)$ is the spatial average over the Gibbs-Boltzmann distribution (see Eq. (8)). Moreover, in Fig. 5(b), one observes that the vertical MSD eventually reaches a plateau at large time lags with a value close to $l_{\rm B}^2$. This saturation corresponds to the fact that the vertical range is limited by gravity, which effectively traps the particle near the bottom wall. The

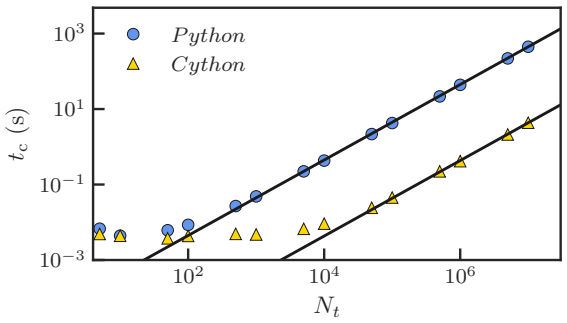

FIG. 4. Real computational times $t_{\rm c}$ as functions of the total number $N_{\rm t}$ of points in a given simulated trajectory, using both *Python* and *Cython*, as indicated. The solid lines correspond to the best linear regressions, from which we find $t_{\rm c}({\rm s}) = 4 \cdot 10^{-5} N_{\rm t}$ for *Python*, and $t_{\rm c}({\rm s}) = 4 \cdot 10^{-7} N_{\rm t}$ for *Cython*.

plateau value can be computed from:

$$\lim_{\tau \to +\infty} \langle \Delta z_t^2 \rangle = \int_{-2H}^{2H} {\rm d}(\Delta z_t) \ \Delta z_t^2 P(\Delta z_t, \tau_\infty) \ , \tag{14}$$

where $P(\Delta z_t, \tau)$ is the Probability Density Function (PDF) of the vertical displacement Δz_t at time lag τ, that tends to $P(\Delta z_t, \tau_\infty)$ when $\tau \to +\infty$ (see Eq. (20)) as discussed in the corresponding section. As shown in Fig. 5, Eqs. (13) and (14) capture well the numerical data, with no free parameter.

B. Fourth-order cumulants in displacements

Beyond the MSDs studied in the previous section, *i.e.* the second-order cumulants of the displacements, one can study higher-order cumulants. Such higher-order cumulants are particularly interesting in order to characterize the inherent non-Gaussianity of the confined Brownian process. The third cumulants $\langle \Delta r_i^3 \rangle_{\rm c}$ are zero, since there is no external drift and $\langle \Delta r_i \rangle = 0$. Therefore, we focus on the fourth cumulants of the displacements:

$$\langle \Delta r_i^4 \rangle_{\rm c} = \langle \Delta r_i^4 \rangle - 3 \langle \Delta r_i^2 \rangle^2 \ . \tag{15}$$

For our class of confined systems (see Fig. 1), in addition to a formal general expression valid at all time lags in the horizontal direction [44], one can derive the short-term and long-term asymptotic behaviors of Eq. (15). At small time lags, one has [44]:

$$\langle \Delta r_i^4 \rangle_{\rm c} \underset{\tau \to 0}{\simeq} 12 \left[\langle D_i^2 \rangle_0 - \langle D_i \rangle_0^2 \right] \tau^2 \ , \tag{16}$$

where the demonstration for the vertical direction is equivalent to the one for the horizontal direction. At large time lags, in the horizontal direction, one has [44]:

$$\langle \Delta x_t^4 \rangle_{\rm c} \underset{\tau \to +\infty}{\simeq} 24 \left(\mathcal{D}_4 \tau - \mathcal{C}_4 \right) , \tag{17}$$

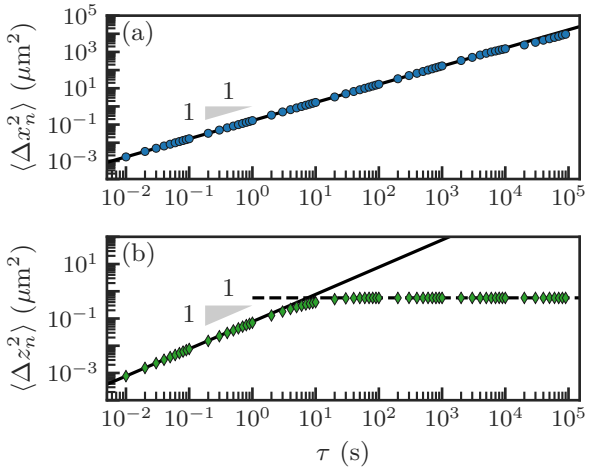

FIG. 5. Mean square horizontal (a) and vertical (b) displacements $\langle \Delta r_{i,n}^2 \rangle$ (see Eq. (12)) as functions of time lag τ, for a simulated trajectory of $N_\mathrm{t} = 10^8$ points, with a numerical time step $\delta t = 0.01$ s. The physical parameters are $a = 1.5$ μm, $B = 5.0$, $l_\mathrm{B} = 526$ nm, $l_\mathrm{D} = 88$ nm and $H_\mathrm{p} = 40$ μm. The solid lines correspond to Eq. (13), and the dashed line to Eq. (14).

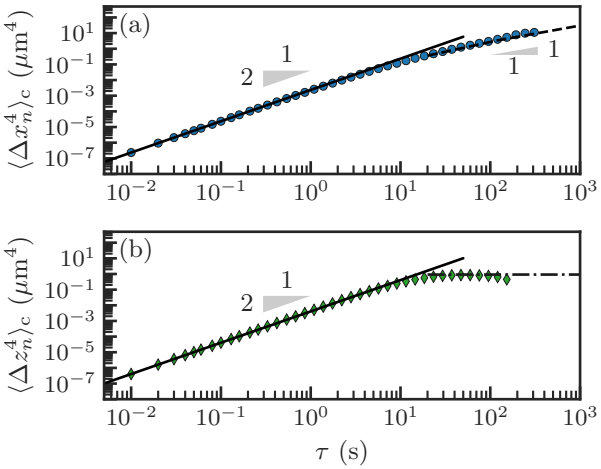

FIG. 6. Fourth cumulants $\langle \Delta r_{i,n}^4 \rangle_\mathrm{c}$ (see Eq. (15)) in horizontal (a) and vertical (b) displacements as functions of time lag τ, for a simulated trajectory of $N_\mathrm{t} = 10^8$ points, with a numerical time step $\delta t = 0.01$ s. The physical parameters are $a = 1.5$ μm, $B = 5.0$, $l_\mathrm{B} = 526$ nm, $l_\mathrm{D} = 88$ nm and $H_\mathrm{p} = 40$ μm. The solid lines correspond to Eq. (16), the dashed line to Eq. (17), and the dash-dotted line to Eq. (18).

where $\mathcal{D}_4$ and $\mathcal{C}_4$ are two known constants depending on V and $\{D_i\}$. At large time lags, in the vertical direction, one expects a plateau given by:

$$\lim_{\tau\to+\infty} \langle \Delta z_t^4 \rangle = \int_{-2H}^{+2H} \mathrm{d}(\Delta z_t)\, \Delta z_t^4 P(\Delta z_t, \tau_\infty) - 3 \left[\int_{-2H}^{+2H} \mathrm{d}(\Delta z_t)\, \Delta z_t^2 P(\Delta z_t, \tau_\infty) \right]^2 , \tag{18}$$

where $P(\Delta z_t, \tau_\infty)$ is defined in Eq. (20), as discussed in the next section.

As shown in Fig. 6, the fourth cumulants in displacements obtained from the numerical simulations are in agreement with the asymptotic expressions of Eqs. (16) to (18), with no adjustable parameter. Moreover, we stress that the fourth cumulant in horizontal displacement depends on both $D_x(z)$ and $D_z(z)$ at long times [44]. As such, there is an information coupling between the vertical and horizontal motions, despite the respective noises are not correlated. This is a potentially relevant feature towards the practical extraction of vertical quantities from simple horizontal statistics in actual experimental systems. Note that this idea was already exploited for the second cumulant in a different class of confined systems [20].

C. Displacement distributions

Having discussed the second and fourth cumulants of displacements in the two previous sections, we now turn to the full PDFs $P(\Delta r_i, \tau)$ of displacements $\Delta r_i = r_i(t+\tau) - r_i(t)$, at time lag τ. Note that, in the discretized version for numerical simulations, we denote these quantities $P(\Delta r_{i,n}, \tau)$, $\Delta r_{i,n}$, and $\tau = k\delta t$, respectively, with k a positive integer. In the bulk, such PDFs obey the diffusion equation and are classically given by Gaussian distributions, each of zero mean and $2D_0\tau$ variance.

In our confined case, the presence of the walls modifies the Brownian motion to a so-called Brownian-yet-non-Gaussian motion [25–44]. As such, the PDFs of displacements are expected to depart from Gaussian distributions. At all time lags τ for the horizontal direction, and at small time lags for the vertical one, the PDFs of displacements can be obtained from spatial averages $\langle \cdot \rangle_0$ of the local diffusion Green's functions over the Gibbs-Boltzmann distribution [19, 23]:

$$P(\Delta r_i, \tau) = \int_{-2H}^{+2H} \mathrm{d}z\, \frac{P_\mathrm{eq}(z)}{\sqrt{4\pi D_i(z)\tau}} \mathrm{e}^{-\frac{\Delta r_i^2}{4D_i(z)\tau}} . \tag{19}$$

As shown in Fig. 7(a,b,c), the PDFs in displacements obtained from the numerical simulations are in agreement with Eq. (19) with no adjustable parameter, at all time lags for the horizontal direction, and at small time lags for the vertical one. Moreover, we observe a departure from the classical bulk Gaussian distributions, that is more pronounced in the vertical direction. Interestingly, even though these three displacement distributions are

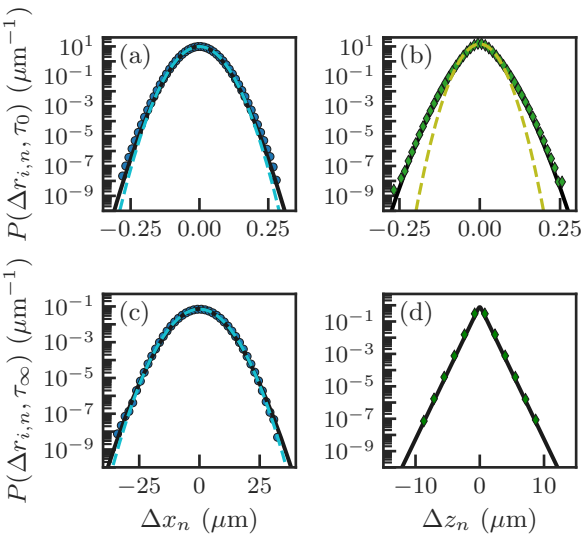

FIG. 7. (a,c) Probability density functions $P(\Delta x_n, \tau)$ in horizontal displacement Δx_n, obtained from numerical simulations (blue dots), at small time lag $\tau_0 = 0.01$ s and large time time lag $\tau_\infty = 95.4$ s, respectively. The solid black lines correspond to Eq. (19), and the dashed blue lines correspond to Gaussian distributions of zero means and $2\langle D_x\rangle\tau$ variances. (b,d) Probability density functions $P(\Delta z_n, \tau)$ in vertical displacement Δz_n, obtained from numerical simulations (green diamonds), at small time lag $\tau_0 = 0.01$ s and large time time lag $\tau_\infty = 95.4$ s, respectively. The solid black lines correspond to Eq. (19), and the dashed green line to a Gaussian distribution of zero mean and $2\langle D_z\rangle\tau$ variance. In all panels, the PDFs are constructed from $N_\mathrm{s} = 2.1 \times 10^6$ trajectories of $N_\mathrm{t} = 10^5$ points each, using a numerical time step $\delta t = 0.01$ s, and the physical parameters: $a = 1.5$ μm, $B = 5.0$, $l_\mathrm{B} = 526$ nm, $l_\mathrm{D} = 88$ nm, and $H_\mathrm{p} = 40$ μm.

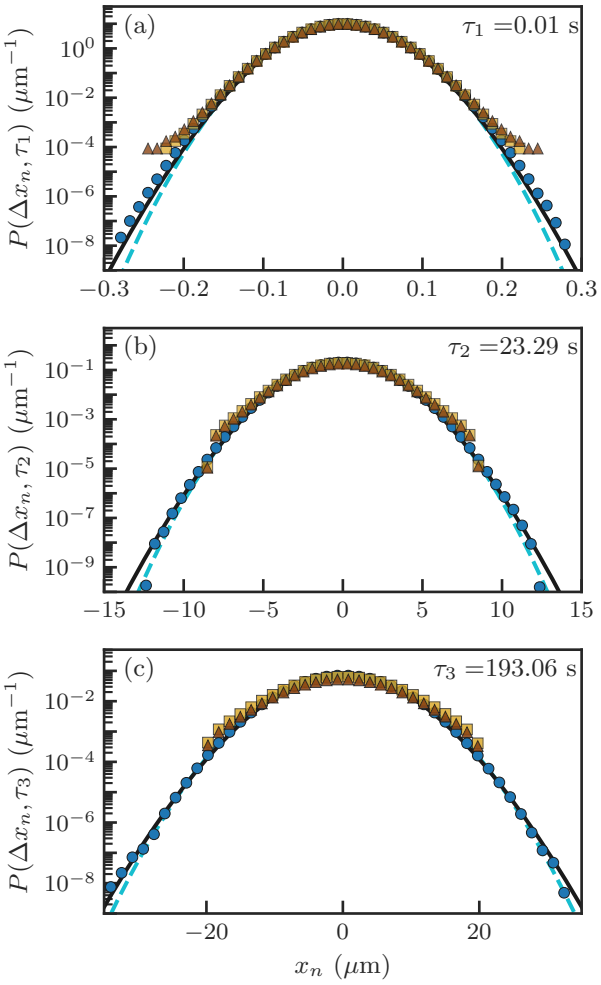

FIG. 8. Probability density functions $P(\Delta x_n, \tau)$ in horizontal displacement Δx_n, obtained from numerical simulations (blue dots) by averaging the individual PDFs of the $N_\mathrm{s} = 2.1 \times 10^6$ trajectories. Three lag times are considered here: (a) $\tau_1 = 0.01$ s, (b) $\tau_2 = 1.09$ s and (c) $\tau_3 = 95.4$ s. For comparison, are shown the data restricted to within the 90^{th} (yellow squares) and 99^{th} (brown triangles) quantiles. The solid black lines correspond to Eq. (19), and the dashed blue lines correspond to Gaussian distributions of zero means and $2\langle D_x\rangle\tau$ variances. In all panels, the PDFs are constructed from trajectories of $N_\mathrm{t} = 10^5$ points each, using a numerical time step $\delta t = 0.01$ s, and the physical parameters: $a = 1.5$ μm, $B = 5.0$, $l_\mathrm{B} = 526$ nm, $l_\mathrm{D} = 88$ nm, and $H_\mathrm{p} = 40$ μm.

non-Gaussian, the corresponding MSDs are still linear in time lag (see Fig. 5), as expected for a Brownian-yet-non-Gaussian process.

Let us now turn to the long-term behaviour of the PDF in vertical displacement. As already observed in Figs. 5 and 6, the second and first cumulants of the vertical displacement reach plateau values at long times. This saturation indicates that equilibrium is reached in the vertical direction. Therefore, one can derive the long-term distribution $P(\Delta z_t, \tau_\infty) \equiv \lim_{\tau\to+\infty} P(\Delta z_t, \tau)$ from the Gibbs-Boltzmann distribution (see Eq. (8)), as [19, 23]:

$$P(\Delta z_t, \tau_\infty) = \int_{-2H}^{+2H} \mathrm{d}z \; P_\mathrm{eq}(z) P_\mathrm{eq}(z + \Delta z_t) \; . \qquad (20)$$

Stated simply, at equilibrium, a certain displacement Δz_t corresponds to having a certain starting point z and the arrival one $z+\Delta z_t$, both being independently distributed according to the Gibbs-Boltzmann distribution, and with a summation over all possible starting points. As shown in Fig. 7(d), the long-term PDF in vertical displacement obtained from the numerical simulations is in agreement with Eq. (20), with no adjustable parameter. Moreover, we observe a marked departure from the classical bulk Gaussian distribution.

D. Rare events and convergence

As seen in Fig. 7(a,c), resolving the non-Gaussianities in the distribution of the horizontal displacement implies to measure large displacements, which are rare events,

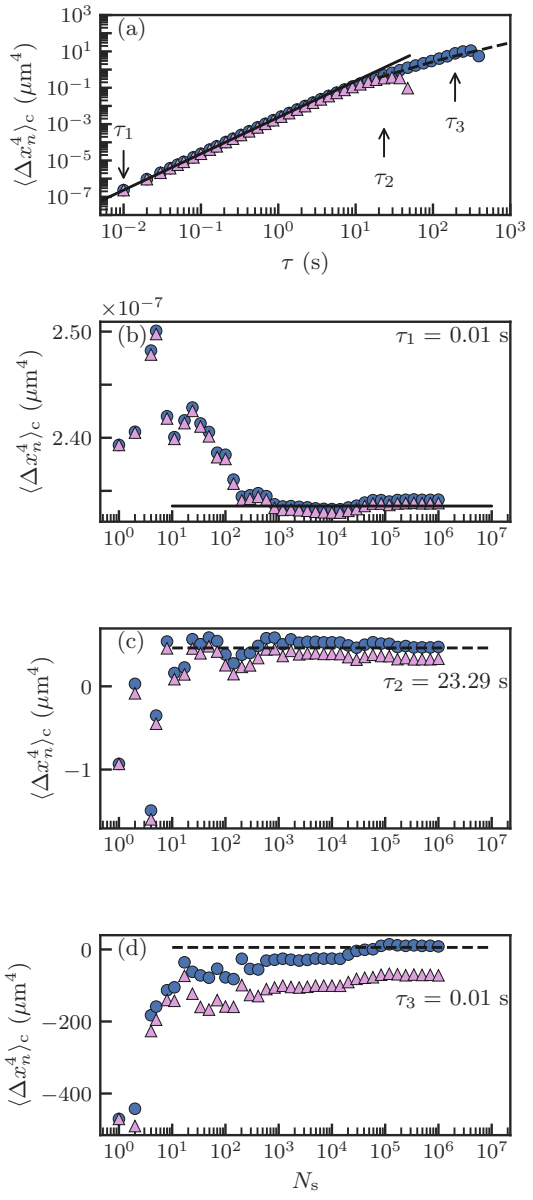

FIG. 9. (a) Fourth cumulant $\langle \Delta x_n^4 \rangle_c$ in horizontal displacement Δx_n as a function of time lag τ, as obtained from the distribution method of Eqs. (21) and (22) (blue circles). For comparison, we also show simple averages (pink triangles) of the fourth cumulants in horizontal displacement obtained from the individual trajectories. (b-d) Fourth cumulants $\langle \Delta x_n^4 \rangle_c$ as functions of the number N_s of simulations, for three different time lags as indicated. In all panels, the solid lines correspond to the short-term asymptotic expression of Eq. (16), and the dashed lines to the long-term asymptotic expression of Eq. (17). The trajectories have $N_t = 10^5$ points each, and the numerical time step is $\delta t = 0.01$ s. The physical parameters in the simulation are: $a = 1.5$ μm, $B = 5.0$, $l_B = 526$ nm, $l_D = 88$ nm, and $H_p = 40$ μm.

and thus require a lot of numerical data. This is illustrated in Fig. 8, where we see that the non-Gaussian data of interest lies outside the 99$^{\text{th}}$ quantiles. As a direct consequence, a single short trajectory does not allow one to resolve the horizontal non-Gaussianities, and thus the fourth cumulant in horizontal displacement. One possible strategy to overcome this issue would be to generate a much longer trajectory, *e.g.* of $N_t = 10^8$ points, but this would be at the expense of accumulating important numerical errors on the rare events. In order to circumvent such an error accumulation, we instead simulate $N_s = 2.1 \times 10^6$ shorter trajectories of $N_t = 10^5$ points each. Note that such an issue is however unimportant for the MSD (see Fig. 5) which is dominated by frequent Gaussian-like events. Therefore, the horizontal MSD can be calculated with a single trajectory of $N_t = 10^8$ points, as in Fig. 5.

Another important practical point to consider is the difficulty in registering $N_s \times N_t$ points, in order to produce the fourth cumulants at large time lags in Fig. 6. To circumvent this issue, we invoke the equivalent expression of the fourth cumulant:

$$\langle \Delta x_t^4 \rangle_c = \int_{-2H}^{+2H} \mathrm{d}(\Delta x_t)\, \Delta x_t^4 P(\Delta x_t, \tau) - 3 \left[\int_{-2H}^{+2H} \mathrm{d}(\Delta x_t)\, \Delta x_t^2 P(\Delta x_t, \tau) \right]^2 . \quad (21)$$

From this expression, we see that one just needs to construct $P(\Delta x_n, \tau)$ from all the numerical trajectories, in order to evaluate $\langle \Delta x_t^4 \rangle_c$. The construction of $P(\Delta x_n, \tau)$ is performed by averaging the PDFs $P^{(k)}(\Delta x_n, \tau)$ of horizontal displacements for the individual trajectories (indexed by the integer k), as:

$$P(\Delta x_n, \tau) = \frac{1}{N_s} \sum_{k=1}^{N_s} P^{(k)}(\Delta x_n, \tau) . \quad (22)$$

In Fig. 9(a), we plot the fourth cumulant in horizontal displacement as a function of time lag, as obtained from this distribution method. For comparison, we also plot the fourth cumulant in horizontal displacement estimated by a naive method, which consists in simply averaging the fourth cumulants in horizontal displacement obtained from the individual trajectories. At small time lags, where single trajectories are sufficient, both methods work properly. At large time lags, the distribution method is still robust, while the naive method underestimates the fourth cumulant. This is intimately rooted in the fact that, as τ increases, single trajectories do not register enough rare events, which are however essential for measuring non-Gaussianities, as discussed above. As shown in Fig. 9(b-d), increasing N_s does not solve the problem with the naive method, which fails in converging to the good value at large time lags. In contrast, the distribution method converges properly in the considered N_s and τ ranges, and is thus more robust.

IV. CONCLUSION

We have numerically investigated the Brownian motion of a negatively-buoyant colloidal particle confined between two flat rigid walls, in presence of surface charges. Specifically, we have solved the discretized overdamped Langevin equation, with an appropriate spurious drift. From the generated trajectories, and with specific care provided regarding the slow convergence of high-order cumulants, we have constructed all the relevant statistical observables. From these, we have in particular checked the convergence to equilibrium, and have quantitatively addressed the non-Gaussianity of the process. As such, our method provides efficient, broadrange and quantitative numerical simulations of Brownian motion in confinement, with potential interest for nanophysics and biophysics.

V. ACKNOWLEDGMENTS

The authors thank Arthur Alexandre, Nicolas Fares, Yann Louyer, Thomas Guérin and David Dean, for interesting discussions. They acknowledge financial support from the European Union through the European Research Council under EMetBrown (ERC-CoG-101039103) grant. Views and opinions expressed are however those of the authors only and do not necessarily reflect those of the European Union or the European Research Council. Neither the European Union nor the granting authority can be held responsible for them. The authors also acknowledge financial support from the Agence Nationale de la Recherche under EMetBrown (ANR-21-ERCC-0010-01), Softer (ANR-21-CE06-0029), and Fricolas (ANR-21-CE06-0039) grants. Finally, they thank the Soft Matter Collaborative Research Unit, Frontier Research Center for Advanced Material and Life Science, Faculty of Advanced Life Science at Hokkaido University, Sapporo, Japan.

[1] Robert Brown. A brief account of microscopical observations made in the months of June, July and August 1827, on the particles contained in the pollen of plants; and on the general existence of active molecules in organic and inorganic bodies. *The Philosophical Magazine*, 4(21):161–173, September 1828.

[2] Albert Einstein. über die von der molekularkinetischen Theorie der Wärme geforderte Bewegung von in ruhenden Flüssigkeiten suspendierten Teilchen. *Annalen der physik*, 4, 1905.

[3] William Sutherland. A dynamical theory of diffusion for non-electrolytes and the molecular mass of albumin. *The London, Edinburgh, and Dublin Philosophical Magazine and Journal of Science*, 9(54):781–785, June 1905.

[4] M. von Smoluchowski. Zur kinetischen Theorie der Brownschen Molekularbewegung und der Suspensionen. *Annalen der Physik*, 326(14):756–780, 1906.

[5] Jean Perrin. Mouvement brownien et grandeurs moléculaires. *Le Radium*, 6(12):353–360, 1909.

[6] Paul Langevin. Sur la théorie du mouvement brownien. *C. R. Acad. Sci. (Paris)*, 146:530–533, 1908.

[7] A. Genthon. The concept of velocity in the history of brownian motion. *The European Physical Journal H*, 45:49, 2020.

[8] V. Ardourel. Brownian motion from a deterministic system of particles. *Synthese*, 200:0:1, 2022.

[9] Howard Brenner. The slow motion of a sphere through a viscous fluid towards a plane surface. *Chemical Engineering Science*, 16(3-4):242–251, December 1961.

[10] G. K. Batchelor. Brownian diffusion of particles with hydrodynamic interaction. *Journal of Fluid Mechanics*, 74(1):1–29, March 1976.

[11] X. Bian, C. Kim, and G. E. Karniadakis. 111 years of Brownian motion. *Soft Matter*, 12:6331, 2016.

[12] Luc P. Faucheux and Albert J. Libchaber. Confined Brownian motion. *Physical Review E*, 49(6):5158–5163, June 1994.

[13] E. R. Dufresne, T. M. Squires, M. P. Brenner, and D. G. Grier. Hydrodynamic coupling of two brownian spheres to a planar surface. *Physical Review Letters*, 85:3317, 2000.

[14] B. U. Felderhof. Effect of the wall on the velocity autocorrelation function and long-time tail of brownian motion. *Journal of Physical Chemistry B*, 109:21406, 2005.

[15] L. Joly, C. Ybert, and L. Bocquet. Probing the nanohydrodynamics at liquid-solid interfaces using thermal motion. *Physical Review Letters*, 96:046101, 2006.

[16] H. B. Eral, J. M. Oh, D. van den Ende, F. Mugele, and M. H. G. Duits. Anisotropic and hindered diffusion of colloidal particles in a closed cylinder. *Langmuir*, 26:16722, 2010.

[17] O. Bénichou, A. Bodrova, D. Chakraborty, P. Illien, A. Law, C. Mejia-Monasterio, G. Oshanin, and R. Voituriez. Geometry-induced superdiffusion in driven crowded systems. *Physical Review Letters*, 111:260601, 2013.

[18] J. Mo, A. Simha, and M. G. Raizen. Broadband boundary effects on brownian motion. *Physical Review E*, 92:062106, 2015.

[19] Mpumelelo Matse, Mykyta V. Chubynsky, and John Bechhoefer. Test of the diffusing-diffusivity mechanism using near-wall colloidal dynamics. *Physical Review E*, 96(4):042604, October 2017.

[20] T. R. Strick, J.-F. Allemand, D. Bensimon, A. Bensimon, and V. Croquette. The elasticity of a single supercoiled dna molecule. *Science*, 271(5257):1835–1837, 1996.

[21] U. Bockelmann, Ph. Thomen, B. Essevaz-Roulet, V. Viasnoff, and F. Heslot. Unzipping dna with optical tweez-

ers: High sequence sensitivity and force flips. *Biophysical Journal*, 82(3):1537–1553, 2002.

[22] S. K. Sainis, V. Germain, and E. R. Dufresne. Statistics of particle trajectories at short time intervals reveal fn-scale colloidal forces. *Physical Review Letters*, 99:018303, 2007.

[23] Maxime Lavaud, Thomas Salez, Yann Louyer, and Yacine Amarouchene. Stochastic inference of surface-induced effects using brownian motion. *Phys. Rev. Research*, 3:L032011, Jul 2021.

[24] M. Rieu, T. Vieille, G. Radou, R. Jeanneret, N. Ruiz-Gutierrez, B. Ducos, J.-F. Allemand, and V. Croquette. Parallel, linear, and subnanometric 3d tracking of microparticles with stereo darkfield interferometry. *Science Advances*, 7(6):eabe3902, 2021.

[25] Yilong Han, AM Alsayed, Maurizio Nobili, Jian Zhang, Tom C Lubensky, and Arjun G Yodh. Brownian motion of an ellipsoid. *Science*, 314(5799):626–630, 2006.

[26] Tobias Munk, Felix Höfling, Erwin Frey, and Thomas Franosch. Effective perrin theory for the anisotropic diffusion of a strongly hindered rod. *EPL (Europhysics Letters)*, 85(3):30003, 2009.

[27] Bo Wang, Stephen M Anthony, Sung Chul Bae, and Steve Granick. Anomalous yet brownian. *Proc. Nat. Acad. Sc.*, 106(36):15160–15164, 2009.

[28] Kyriacos C Leptos, Jeffrey S Guasto, Jerry P Gollub, Adriana I Pesci, and Raymond E Goldstein. Dynamics of enhanced tracer diffusion in suspensions of swimming eukaryotic microorganisms. *Phys. Rev. Lett.*, 103(19):198103, 2009.

[29] Bo Wang, James Kuo, Sung Chul Bae, and Steve Granick. When brownian diffusion is not gaussian. *Nature materials*, 11(6):481–485, 2012.

[30] Michael J Skaug, Joshua Mabry, and Daniel K Schwartz. Intermittent molecular hopping at the solid-liquid interface. *Phys. Rev. Lett.*, 110(25):256101, 2013.

[31] Mykyta V Chubynsky and Gary W Slater. Diffusing diffusivity: A model for anomalous, yet brownian, diffusion. *Phys. Rev. Lett.*, 113(9):098302, 2014.

[32] Juan Guan, Bo Wang, and Steve Granick. Even hard-sphere colloidal suspensions display fickian yet non-gaussian diffusion. *ACS nano*, 8(4):3331–3336, 2014.

[33] Rohit Jain and Kizhakeyil L Sebastian. Diffusion in a crowded, rearranging environment. *J. Phys. Chem. B*, 120(16):3988–3992, 2016.

[34] Rohit Jain and Kizhakeyil L Sebastian. Diffusing diffusivity: survival in a crowded rearranging and bounded domain. *J. Phys. Chem. B*, 120(34):9215–9222, 2016.

[35] Aleksei V. Chechkin, Flavio Seno, Ralf Metzler, and Igor M. Sokolov. Brownian yet Non-Gaussian Diffusion: From Superstatistics to Subordination of Diffusing Diffusivities. *Physical Review X*, 7(2):021002, April 2017.

[36] Vittoria Sposini, Aleksei Chechkin, and Ralf Metzler. First passage statistics for diffusing diffusivity. *J. Phys. A: Math Theor*, 52(4):04LT01, 2018.

[37] Yann Lanoiselée, Nicolas Moutal, and Denis S Grebenkov. Diffusion-limited reactions in dynamic heterogeneous media. *Nat. Comm.*, 9(1):4398, 2018.

[38] Yann Lanoiselée and Denis S Grebenkov. A model of non-gaussian diffusion in heterogeneous media. *J. Phys. A: Math. Theor.*, 51(14):145602, 2018.

[39] Paweł Czajka, Jan M Antosiewicz, and Maciej Długosz. Effects of hydrodynamic interactions on the near-surface diffusion of spheroidal molecules. *ACS omega*, 4(16):17016–17030, 2019.

[40] Indrani Chakraborty and Yael Roichman. Disorder-induced fickian, yet non-gaussian diffusion in heterogeneous media. *Phys. Rev. Res.*, 2(2):022020, 2020.

[41] M Hidalgo-Soria and E Barkai. Hitchhiker model for laplace diffusion processes. *Phys. Rev. E*, 102(1):012109, 2020.

[42] Qingqing Yin, Yunyun Li, Fabio Marchesoni, Subhadip Nayak, and Pulak K Ghosh. Non-gaussian normal diffusion in low dimensional systems. *Frontiers of Physics*, 16(3):1–14, 2021.

[43] José M Miotto, Simone Pigolotti, Aleksei V Chechkin, and Sándalo Roldán-Vargas. Length scales in brownian yet non-gaussian dynamics. *Phys. Rev. X*, 11(3):031002, 2021.

[44] Arthur Alexandre, Maxime Lavaud, Nicolas Fares, Elodie Millan, Yann Louyer, Thomas Salez, Yacine Amarouchene, Thomas Guérin, and David S. Dean. Non-Gaussian diffusion near surfaces. *arXiv:2207.01880*, 2022.

[45] S. Marbach, D. S. Dean, and L. Bocquet. Transport and dispersion across wiggling nanopores. *Nature Physics*, 14:1108, 2018.

[46] R. Sarfati, C. P. Calderon, and D. K. Schwartz. Enhanced diffusive transport in fluctuating porous media. *ACS Nano*, 15:7392, 2021.

[47] O. Bénichou, C. Loverdo, M. Moreau, and R. Voituriez. Optimizing intermittent reaction paths. *Physical Chemistry Chemical Physics*, 10:7059, 2008.

[48] Giuseppe Boniello, Christophe Tribet, Emmanuelle Marie, Vincent Croquette, and Dražen Zanchi. Rolling and aging in temperature-ramp soft adhesion. *Phys. Rev. E*, 97:012609, Jan 2018.

[49] A. Alexandre, M. Mangeat, T. Guérin, and D. S. Dean. How stickiness can speed up diffusion in confined systems. *Phys. Rev. Lett.*, 128:210601, May 2022.

[50] T. Bickel. Brownian motion near a liquid-like membrane. *European Physical Journal E*, 20:379, 2006.

[51] G. M. Wang, R. Prabhakar, and E. M. Sevick. Hydrodynamic mobility of an optically trapped colloidal particle near fluid-fluid interfaces. *Physical Review Letters*, 103:248303, 2009.

[52] A. Daddi-Moussa-Ider, A. Guckenberger and S. Gekle. Particle mobility between two planar elastic membranes: Brownian motion and membrane deformation. *Physics of Fluids*, 28:071903, 2016.

[53] Chen Bar-Haim and Haim Diamant. Correlations in suspensions confined between viscoelastic surfaces: Noncontact microrheology. *Phys. Rev. E*, 96:022607, Aug 2017.

[54] C. M. Cejas, F. Monti, M. Truchet, J.-P. Burnouf, and P. Tabeling. Particle deposition kinetics of colloidal suspensions in microchannels at high ionic strength. *Langmuir*, 33:6471, 2017.

[55] Alexandre Vilquin, Vincent Bertin, Pierre Soulard, Gabriel Guyard, Elie Raphaël, Frédéric Restagno, Thomas Salez, and Joshua D. McGraw. Time dependence of advection-diffusion coupling for nanoparticle ensembles. *Phys. Rev. Fluids*, 6:064201, Jun 2021.

[56] A. Vilquin, V. Bertin, E. Raphaël, D.S. Dean, T. Salez, and J.D. McGraw. Nanoparticle taylor dispersion near charged surfaces with an open boundary. *arXiv:2206.07413*, 2022.

[57] Giorgio Volpe and Giovanni Volpe. Simulation of a Brownian particle in an optical trap. *American Journal of Physics*, 81(3):224–230, March 2013.

[58] Sven H. Behrens and David G. Grier. The charge of glass and silica surfaces. *The Journal of Chemical Physics*, 115(14):6716–6721, October 2001.

[59] M. I. M. Feitosa and O. N. Mesquita. Wall-drag effect on diffusion of colloidal particles near surfaces: A photon correlation study. *Physical Review A*, 44(10):6677–6685, November 1991.

[60] Michael A. Bevan and Dennis C. Prieve. Hindered diffusion of colloidal particles very near to a wall: Revisited. *The Journal of Chemical Physics*, 113(3):1228–1236, July 2000.

[61] Hilding Faxen. Die Bewegung einer starren Kugel langs der Achse eines mit zaher Flussigkeit gefullten Rohres. *Arkiv for Matemetik Astronomi och Fysik*, 17:1–28, 1923.

[62] Riccardo Mannella and Peter V. E. McClintock. Itô versus stratonovich: 30 years later. *Fluctuation and Noise Letters*, 11(01):1240010, March 2012.

[63] J. M. Sancho. Brownian colloidal particles: Ito, Stratonovich, or a different stochastic interpretation. *Physical Review E*, 84(6):062102, December 2011.

[64] Makoto Matsumoto and Takuji Nishimura. Mersenne twister: A 623-dimensionally equidistributed uniform pseudo-random number generator. *ACM Transactions on Modeling and Computer Simulation*, 8(1):3–30, January 1998.

[65] David W. Scott. Box–Muller transformation. *WIREs Computational Statistics*, 3(2):177–179, 2011.

[66] D.-U. Lee, J.D. Villasenor, W. Luk, and P.H.W. Leong. A hardware Gaussian noise generator using the Box-Muller method and its error analysis. *IEEE Transactions on Computers*, 55(6):659–671, June 2006.

[67] Luc Devroye. *Non-Uniform Random Variate Generation*. Springer, New York, NY, 1986.

[68] Guido Van Rossum and Fred L Drake Jr. *Python Tutorial*. Centrum voor Wiskunde en Informatica Amsterdam, The Netherlands, 1995.

[69] Stefan Behnel, Robert Bradshaw, Craig Citro, Lisandro Dalcin, Dag Sverre Seljebotn, and Kurt Smith. Cython: The Best of Both Worlds. *Computing in Science & Engineering*, 13(2):31–39, March 2011.

[70] C. L. Vestergaard, J. N. Pedersen, K. I. Mortensen, and H. Flyvbjerg. Estimation of motility parameters from trajectory data. *The European Physical Journal Special Topics*, 224(7):1151–1168, July 2015.